Thermal analysis and shrinkage characterization of the photopolymers for DLP additive manufacturing processes

Kubra Sekmen, Thomas Rehbein, Michael Johlitz, Alexander Lion, Andrei Constantinescu

Thermal analysis and shrinkage characterization of the photopolymers for DLP additive manufacturing processes

Kubra Sekmen[1], Thomas Rehbein[2], Michael Johlitz[2], Alexander Lion[2] and Andrei Constantinescu[1*]

[1*]Laboratoire de Mécanique des Solides, CNRS, École Polytechnique, Institut Polytechnique de Paris, 91128, Palaiseau, France.

[2]Department of Aerospace Engineering, Institute of Mechanics, Bundeswehr University Munich, Werner-Heisenberg-Weg 39, 85577, Neubiberg, Germany.

*Corresponding author(s). E-mail(s): andrei.constantinescu@polytechnique.edu;
Contributing authors: kubra.sekmen@polytechnique.edu; rehbein@unibw.de; michael.johlitz@unibw.de; alexander.lion@unibw.de;

Abstract

This paper proposes an experimental investigation of a commercial photopolymer resin followed by material modelling and manufacturing system characterization. We focus on the effect of the degree of cure and temperature on the material properties of the photopolymer materials. UV curing properties of the liquid resin are assessed with the thickness measurement by optical tomography. Besides, the specific heat capacity is determined for the almost completely cured and uncured samples with DSC measurements. Photo-DSC experiments are performed to investigate the curing reaction and modelling of the evolution of the degree of cure depending on the light intensity and temperature. In addition, chemical shrinkage behaviour is captured as function of the degree of cure by the high-precision balance setup. As a result of our experimental studies, model equations are proposed to describe the material behaviour.

Keywords: Additive manufacturing, Photopolymerization, UV curing, Digital light processing

1 Introduction

Additive manufacturing (AM) technology opens up new possibilities for the rapid production of polymer parts in comparison to conventional manufacturing methods, combining the high geometrical flexibility with high resolution. Among AM technologies, digital light processing (DLP) 3D printing is one of the innovative fabrication methods that builds 3D objects with complex geometry in a layer-by-layer fashion through simultaneous in-plane photopolymerization [1]. Due to the advantages of high printing speed [2, 3] and high manufacturing precision [4, 5], DLP 3D printing has been extensively utilized in various industrial applications such as dental technology [6, 7], microfluidic devices [8–10], jewellery manufacturing and fashionwear [11, 12], tissue engineering [13, 14], metamaterials [15, 16], engineered nerve guidance conduits [14, 17] and electrically conductive structures [18, 19].

3D printing based on UV curing is particularly interesting for the growth of industrial applications because high-resolution can be obtained at ambient temperature while consuming less energy and taking up less space in addition to a broad range of resin formulations. UV curing progress during the photopolymerization reaction is outlined in Figure 1. In the beginning ($t = t_0$), the photopolymer resin is in the liquid state and commonly contains uncured monomers, oligomers and photoinitiators. By exposing the liquid resin to UV light ($t = t_1$), the photoinitiators are activated and the photocuring reaction is initiated [1]. Activated photoinitiators crosslink monomers and oligomers, increasing the viscosity during the phase transition from a liquid to a solid, and the gelled resin solidifies within a few seconds ($t = t_2$). Subsequently, a crosslinked three-dimensional network forms a stiff polymer at the end of the curing reaction ($t = t_3$) [20]. The schematic of a digital light processing (DLP) 3D printing system, in which photopolymerization is used for fabrication, is depicted in Figure 2. In DLP 3D printing, a grayscale pixelated Portable Network Graphics (PNG) image of the desired 3D model represents a photomask for the corresponding entire layer [20, 21]. The UV LED light source projects a custom-patterned PNG image onto the 2D plane according to the printing parameters, and sends it to the expanding optics to create a layer of the 3D part. These expanding optics distribute UV light homogeneously into the digital micromirror device (DMD) in order to direct the incoming light distribution through the PDMS window to the liquid photopolymer resin in the resin tray (vat). The exposed liquid polymer cures and attaches to the build head, and then the build head moves upwards a distance equal to the layer thickness to print the next layer. These steps are repeated until the printing of the 3D model is complete.

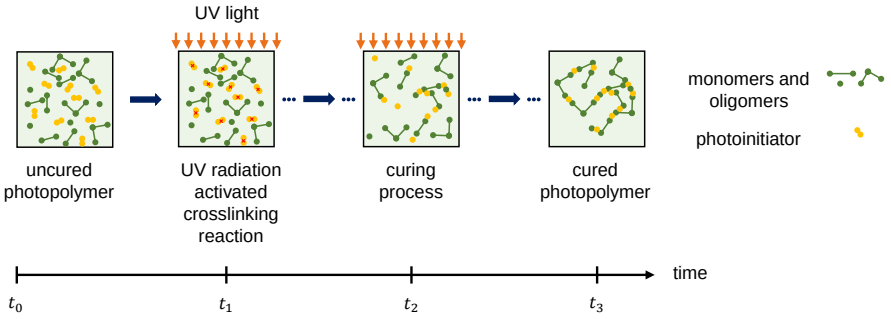

Fig. 1 Schematic representation of the photopolymerization reaction in the material unit cell.

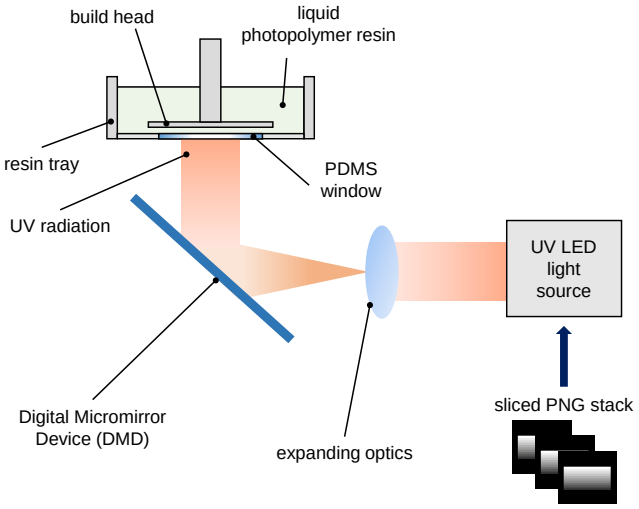

Fig. 2 Schematic of a digital light processing (DLP) 3D printer.

During 3D printing, the degree of cure increases due to the change in the crosslinking density depending on the process parameters [22, 23]. This increase in the degree of cure leads to changes in the final product properties such as tensile strength and Young's modulus [24, 25], viscoelastic properties [22, 23, 26], volumetric shrinkage [27, 28], specific heat capacity [29, 30], and glass transition temperature [31, 32]. Volumetric shrinkage due to the coupling of several phenomena such as non-uniform UV light absorption in the liquid resin medium and heterogeneity in the photopolymerization causes residual stress build-up and thus warping or shape distortion of the printed material. These phenomena combined with layer-by-layer printing result in many challenges such as insufficient repeatability and consistency in the printed products to be addressed [22, 33]. It is a big challenge to develop a complete model that includes all of the aforementioned features needed to simulate photopolymer

curing processes. Therefore, reliable and experimentally validated constitutive models are required for the numerical simulations to predict the material behaviour during and after the printing process.

To fill this gap, our objective is to combine experimental investigations as well as material modelling techniques to predict the influence of the process parameters on the final product properties. In this study, a commercial photosensitive resin is used for material characterization. 3D objects are fabricated by curing in a UV chamber and printing with a DLP 3D printer. We study the effect of UV light intensity, temperature and exposure time on the degree of cure-dependent material properties. The UV curing properties of the resin are first determined by the working curve approach. Photocalorimetric measurements of the liquid resin are performed to model the evolution of the degree of cure. Calorimetric measurements are used to determine the specific heat capacity of the material as a function of temperature and degree of cure. Furthermore, the chemical shrinkage induced by the photopolymerization is assessed by density measurements. Model equations are provided to describe the material behaviour as a consequence of our experimental findings.

2 Material and methods

2.1 Material

The material under scrutiny is a commercial standard clear PR48 resin from Colorado Photopolymer Solutions (Boulder, CO, USA). The PR48 is an acrylate-based photopolymer resin working with DLP and stereolithography apparatus (SLA) 3D printing technologies [34].

PR48 is composed of two oligomers, a photoinitiator, a reactive diluent, and a UV blocker [35, 36]. The chemical reaction of PR48 is free-radical polymerization where UV light is used to initiate the crosslinking process, thereby growing the polymer chain. Table 1 gives the summary of the formulation of PR48 resin. The oligomers of this resin are Allnex Ebecryl 8210 (39.776 wt%) and Sartomer SR 494 (39.776 wt%). Ebecryl 8210 is an aliphatic urethane acrylate that has a high molecular weight with low viscosity and high reactivity to UV light irradiation. Sartomer SR 494 is an alkoxylated pentaerythritol tetraacrylate. It is a multifunctional acrylic monomer that enables the polymerization reaction with enriched double bonds. PR48 contains a monofunctional urethane acrylate, Rahn Genomer 1122 (19.88 wt%), as a reactive diluent to reduce the viscosity. Reacting with the other chemical components of the resin, it optimizes the final properties of the printed samples. Esstech TPO+ (0.4 wt%) is the photoinitiator of the resin that initiates the crosslinking reactions of the monomers and oligomers upon UV light exposure. The UV blocker of this resin is Mayzo OB+ (0.16 wt%), 2,2-(2,5-thiophenediyl)bis(5-tertbutylbenzoxazole), which governs the UV light penetration depth to restrict the layer thickness.

Table 1 Formulation of PR48 resin.

	Ingredient	%	Function
Reactive oligomers	Allnex Ebecryl 8210 (Aliphatic urethane acrylate)	39.776	Crosslinking
	Sartomer SR 494 (Alkoxylated pentaerythritol tetraacrylate)	39.776	
Reactive diluent	Rahn Genomer 1122 (Monofunctional urethane acrylate)	19.888	Crosslinking
Photoinitiator	Esstech TPO+ (2,4,6 Trimethylbenzoyl diphenyl phosphineoxide)	0.400	Polymerization: Initiation
UV-blocker	Mayzo OB+ (2,2'-(2,5 thiophenediyl) bis (5-tertbutylbenzoxazole))	0.160	UV light penetration control

2.2 Manufacturing platforms

In this study, two manufacturing platforms were used for the preparation of the samples, depending on the purposes of the experiments.

An open-source Ember DLP 3D printer (Autodesk, San Rafael, CA, USA) was used to fabricate thin-film samples for the characterization of the UV curing properties. The light source of this printer has an LED with a maximum optical power of 5 W and a wavelength of 405 nm. The printer has a resolution of 50 × 50 µm^2 which corresponds to the projection of a single image pixel. Depending on the resin composition and printing settings, the layer thickness varies from 10 to 100 µm. The printer has a maximum build size of 64 × 40 × 134 mm^3, which corresponds to a 1280 × 800 pixels resolution in the PNG images. This open-source system permits the adjustment of the process parameters.

In addition, a UV chamber with the product name UVP Crosslinker CL-1000L (Analytik Jena AG, Jena, Germany) with a 365 nm UV light source was utilized to cure liquid resin between clamped glass slides separated by Teflon molds.

2.3 Irradiance characterization

The material properties of photopolymer materials are significantly affected by the UV lamp system used for curing. One of the most important aspects of UV exposure is UV irradiance (or intensity). Therefore, the UV irradiances of both the UVP Crosslinker and the Ember DLP 3D printer were monitored using a Model 222 light meter (G&R Labs, Santa Clara, CA, USA) equipped with probes for 365 nm and 405 nm wavelengths, respectively.

Two sets of measurements were carried out to determine the UV light intensity of the Ember 3D printer. In both measurements, the UV light source output was monitored in the energy dose mode using the relationship:

$$E_0 = \mathcal{I}_0 t \tag{1}$$

where E_0 denotes the UV energy dose in mJ/cm^2 at the measurement surface during the exposure time t in seconds and $\mathcal{I}_0$ is the UV light intensity in mW/cm^2. The objective of the first measurement is the verification of the constant light intensity during UV radiation of the Ember printer. Accordingly, eight levels of UV dose were applied with exposure times ranging from 1 to 8 seconds. The UV light energy was measured at different horizontal positions on the PDMS window for each UV exposure. The second experiment was conducted to assess the UV light intensity during the fabrication of thin films used for the determination of the UV curing properties presented in Section 2.4 and the working curve of the photopolymer resin analyzed in Section 3.2. Following the method similar to the previous experiment, the measurement was performed on the glass microscope slide (Corning®) with a thickness of 0.9 mm, which was placed on the PDMS window in order to print the thin layer.

For the measurement of the UV light intensity of the UVP Crosslinker, the photometer probe was placed relative to the position of the samples for curing. The glass slide used for the curing reaction was placed on the probe to measure the light intensity received by the photopolymer liquid resin between the clamped glass slides.

2.4 UV curing properties

Photopolymer resins are liquid media that allow UV light penetration. The attenuation of light passing through the resin is a key phenomenon in the photopolymerization reaction [37]. The loss in light intensity caused by absorption or scattering is referred to as attenuation. As a result, the amount of UV light intensity decreases in the printing direction as the depth passed through the medium increases. It is therefore essential to understand the properties of the liquid photopolymer resin to select the printing settings required to obtain desired final product features.

The Beer-Lambert law describes this light attenuation in the medium by a decreasing exponential function of the distance z [38]:

$$\mathcal{I}(z) = \exp\left(-\frac{z}{D_p}\right)\mathcal{I}_0 \tag{2}$$

$\mathcal{I}(z)$ is the light intensity as a function of distance z and D_p denotes the penetration depth z at which the intensity has reduced to a factor e^{-1}. Figure 3 shows the attenuation according to the Beer-Lambert law. The layer height and interfacial strength between successive layers are controlled by the penetration depth D_p, which is a feature of the material's specific composition. In order to build a curing process model, Jacobs [39] developed the working curve equation for a stereolithography process based on the Beer-Lambert absorption law:

$$C_d = D_p \ln\left(\frac{E_0}{E_c}\right) \tag{3}$$

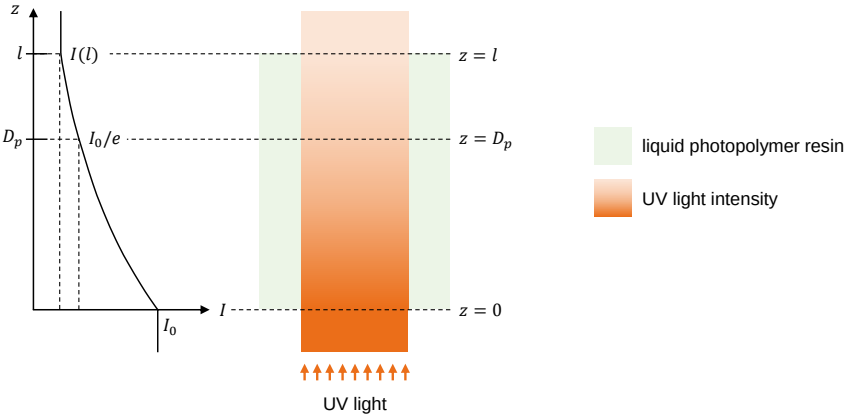

Fig. 3 Beer-Lambert attenuation of UV light intensity with respect to the travelled path in the liquid resin medium ($\mathcal{I}_0$: incident light intensity, D_p: penetration depth at which the light intensity drops to e^{-1}, l: thickness of photopolymer liquid resin in order of 10-100 micrometers).

where C_d is the thickness of a cured layer after the UV light irradiation, known as the cure depth, and E_c is the critical exposure energy required to solidify the photopolymer at its gel point. The gel point is defined as the state in which the resin undergoes a phase transition from the liquid to the solid state with a sudden increase in viscosity [37]. The expression given in Equation 3 corresponds to a linear line on a semi-log plot of C_d-E_0 for the working curve of a specific material where D_p is the slope and E_c is the horizontal axis intercept. This working curve method is used to study the curing behaviour of specific resin compositions in order to evaluate the amount of UV light energy required to cure a liquid photopolymer to the desired layer thickness.

In order to plot the working curve, single-layer samples with different cure depths C_d were printed by applying different UV exposure doses. To print these layers, a UV transparent microscope glass slide was placed on the PDMS window of the Ember DLP 3D printer, as can be seen in Figure 4. As mentioned in Section 2.3, the UV light intensity was measured by a light meter. Following the method of Shah et al. [40], single-layer films were printed on the glass slide at a constant light intensity by choosing exposure times of 4, 6, 8, 10, 12, 14 and 16 s. Three samples were printed for each UV exposure dose to ensure reproducibility. Once the printing step was finished, the printed single-layers attached to the glass slide and excess photopolymer resin were rinsed with isopropanol (IPA) washing through an ultrasonic cleaner for 15 seconds. After the IPA was evaporated, all the samples were vacuumed and sealed inside a moisture-barrier bag and stored in a refrigerator at 5 °C in order to avoid interaction with any other medium such as air, daylight, moisture, or temperature until the day of the experiment.

The thickness of the cured samples was measured using a Ganymade^{TM} spectral-domain optical coherence tomography (SD-OCT) (Thorlabs, Newton,

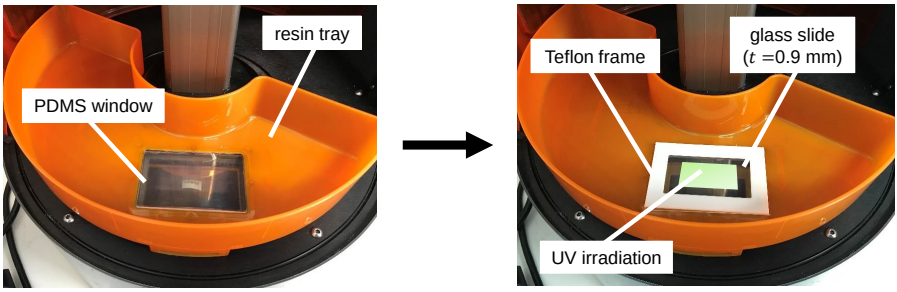

Fig. 4 Layer curing protocol. Left: Resin tray (vat) of Ember DLP 3D printer. Right: Experimental setup for the single-layer printing with representative UV light irradiation.

NJ, USA) with an operating central wavelength of 930 nm. The Ganymede SD-OCT has an axial resolution of <5.8 µm in air and a lateral resolution of 8 µm. Two-dimensional scans were acquired over time with a scanning rate of 10 kHz. The 2D OCT scans of 1124 × 1024 pixels correspond to a scanned area of 8.36 × 2 mm^2 (with a pixel size of 7.67 × 1.95 μm^2). Due to the limited scanning area of the SD-OCT, it is not possible to scan the complete layer at once. Therefore, all samples were scanned at least four times. The visualization of the 2D OCT scans and measurements were employed using the Fiji open-source software [41]. As can be seen in Figure 5, the cure depth C_d was measured away from the edges of the sample. Furthermore, it has been observed that bending occurred in the single printed layer due to buckling or chemical shrinkage indicating the presence of residual strain. In this OCT scan, the upper surface of the cured film, which is seen as the upper curved line, is the surface where it contacts the glass slide in Figure 4, which is more exposed to the UV light, and the surface in contact with the substrate is the surface that is exposed to less UV light due to the exponential attenuation of the UV light intensity. Therefore, according to the position of the cured film in Figure 5, the upper surface has a higher degree of cure than the lower surface, and this leads to the build-up of the residual stresses because of the difference in the chemical shrinkage. This will be investigated in future studies.

2.5 Calorimetric measurements

Liquid monomers and oligomers are converted to solid polymers by crosslinking reactions initiated by heat or exposure to UV radiation. This implies an exothermic reaction of the monomers that are linked to polymer chains. Differential scanning calorimetry (DSC) can analyze the heat released to establish a connection between temperature and specific physical properties. In this work, a heat-flux type DSC 214 Polyma (Netzsch, Selb, Germany) was employed for the characterization of the onset temperature of thermal curing and the specific heat capacity of the PR48 material. Photo-DSC has been commonly used to identify the key process parameters of photopolymerization such as the

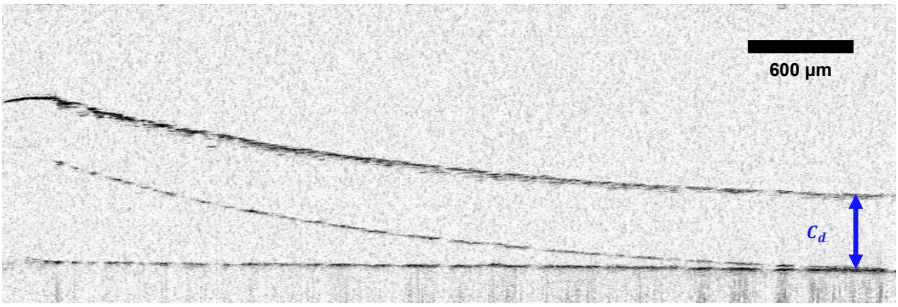

Fig. 5 Lateral image of a single-layer by SD-OCT. The cured layer had an exposure time of 16 s and a thickness of $C_d = 510$ µm.

degree of cure, photopolymerization rate and reaction enthalpy as a function of UV light intensity, exposure time and temperature [42–44]. Photocalorimetric measurements were performed in a heat-flux type DSC Q2000 (TA Instruments, New Castle, DE, USA) to measure the heat of polymerization and to model the crosslinking reaction. Figure 6 depicts a schematic representation of a heat-flux conventional DSC and heat-flux photo-DSC. During the endothermic/exothermic process initiated by the temperature and/or the UV light, heat flow from the furnace to the sample crucible is different from that from the furnace to the reference crucible. DSC analyzes the incoming or outgoing specific heat flux $\dot{h}(t)$ of a sample by comparing it to an empty reference crucible.

The experimentally determined degree of cure $q(t)$ is defined by the conversion of specific heat flow $\dot{h}(t)$ divided by the total heat of reaction h_{tot} measured by combining irradiation and heating, as given in the following equation:

$$q(t) = \frac{\int_0^t \dot{h}(\tilde{t})\mathrm{d}\tilde{t}}{h_{\text{tot}}} \tag{4}$$

The degree of cure is a non-dimensional quantity ranging from 0 (liquid monomer) to 1 (fully cured solid polymer). This relationship was used for the modelling of the reaction kinetics and determining the degree of cure for the samples used in chemical shrinkage tests.

Before starting experiments in which temperature is a variable parameter, isothermal DSC tests were run to demonstrate that the material will not thermally polymerize below the onset temperature of thermal curing. The isothermal DSC test of the liquid resin samples weighing between 10 and 14 mg was performed with the DSC 214 Polyma for 3 hours. Nitrogen was used as a purge gas with a flow rate of 40 ml/min. As can be seen in Figure 7, all experiments (photo-DSC, specific heat capacity measurements) should be carried out below 165 °C to avoid thermal polymerization. Moreover, it should be noted that the glass transition temperature of the liquid photopolymer resin was observed at $T_g = -58.13$ °C.

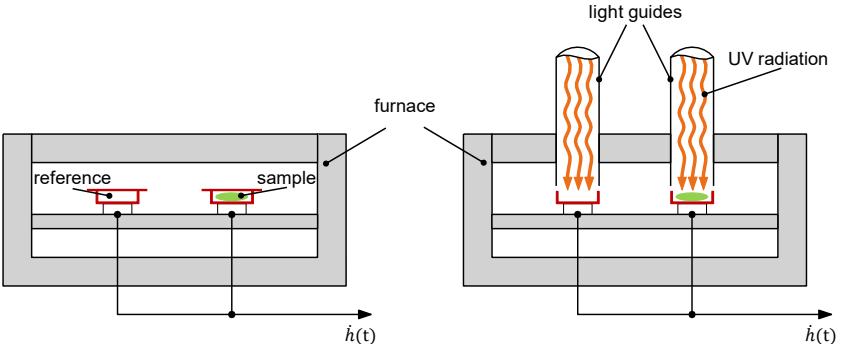

Fig. 6 Schematic diagram of conventional heat-flux DSC (left) and photo-DSC (right) measurement cells.

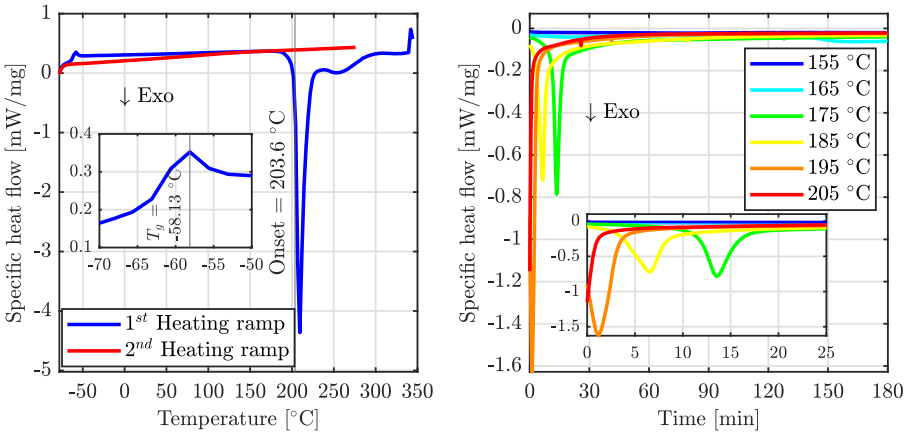

Fig. 7 Determination of the onset temperature of thermal curing. Left: Fast DSC scanning at a heating rate of 10 K/min to limit the upper temperature for the isothermal DSC runs. Right: A set of isothermal DSC runs to demonstrate that the thermal curing of PR48 photopolymer resin is not initiated below 165 °C at a time scale of 180 min.

2.5.1 Photocalorimetric measurements

In order to investigate the curing kinetics of the PR48 photopolymer resin, photocalorimetric measurements were conducted in a DSC Q2000 equipped with an additional light source, OmniCure® S2000 (Excelitas, Waltham, MA, USA). This light source has a 200 W high-pressure mercury lamp and a standard filter with a wavelength of 405 nm. The UV light is transmitted to the sample chamber via a dual-quartz light guide. The Tzero® technology of the DSC enables direct light intensity monitoring at both the sample and the reference positions. Standard DSC measurements for the characterization of the crosslinking mechanisms of polymers require a considerable amount of the sample (5-15 mg). However, the curing progress of the photopolymer sample is sensitive to the chosen mass in the photo-DSC measurements. This behaviour is caused by the exponential attenuation of the incident irradiation according to

the Beer-Lambert law while passing through the liquid photopolymer medium, as explained in Section 2.4. If the sample mass is too high, the thickness of the sample inside the DSC pan will also increase. This increase in thickness affects the exponential attenuation of the UV light and the sample crosslink is formed inhomogeneously through the thickness. To avoid this effect, samples weighing 1.12-1.51 mg were placed in uncovered aluminum pans, which corresponds to the standard layer thickness in DLP 3D printing (50 μm), under nitrogen at a flow rate of 50 ml/min as a purge gas. For the measurement of specific heat flow $\dot{h}(\tilde{t})$ in Equation 4, photo-DSC tests were carried out as follows: (i) a 2 minutes stabilization step of the measurement cell under a specific constant temperature (θ = 10, 20, 30, 40, 50 and 60 °C), (ii) irradiation of the specimen for 10 minutes at a constant UV light intensity ($\mathcal{I}_0$ = 5, 10 mW/cm^2) under isothermal condition, (iii) a final isothermal step of 2 minutes under the specific constant temperature. At each isothermal test, the curing reaction was considered as finished for a given temperature and incident light intensity when the heat flow curve remained stable over time. After completing the procedure, these three steps were repeated with the polymerized sample to generate the baseline heat flow resulting from the UV absorption between the reference aluminum pan and the polymerized sample [45]. This generated baseline was subtracted from the heat flow signal of the first measurement to remove the effect of the UV light source.

The series of photopolymerization measurements are presented in Figure 8 after subtraction of the baseline. It can be seen that the photopolymerization reaction takes place very fast and that the specific heat flow attains its maximum level only a few seconds after the onset of UV light irradiation. Furthermore, as the curing temperature increases, the exothermic peak becomes more significant, which leads to a higher degree of cure. Similarly, higher light intensity results in higher exothermic peaks.

For the measurement of the total specific heat of reaction h_{tot}, the photo-DSC runs were first kept isothermally for 2 minutes at 60 °C and then exposed to the UV light with the intensity of 20 mW/cm^2 for 10 minutes under isothermal conditions. Next, an additional non-isothermal step with the same continuous and constant UV irradiation was performed from 60 °C to 120 °C with a heating rate of 20 °C/min. The final step was to run an isothermal DSC scan at 120 °C for 2 minutes without UV irradiation. The resulting specific heat flow of this procedure is presented by the blue curve in Figure 9. Finally, the same test procedure was repeated with the crosslinked polymer, which is represented by the red curve in the specific heat flow plot over time. By calculating the accumulated area between the red and the blue curve, the total specific heat of reaction was found to be $h_{tot} = -404.43$ J/g. For all measurements, this value is taken as reference value for the determination of the degree of cure in Section 3.3.

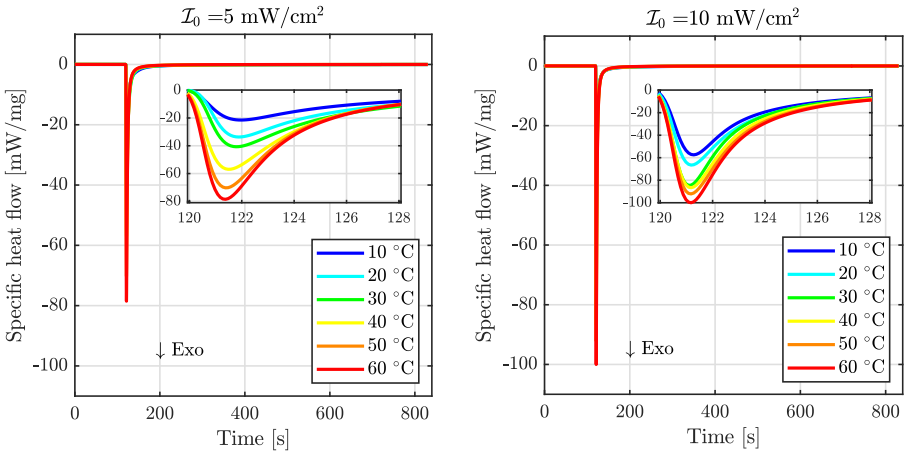

Fig. 8 Photo-DSC measurements of specific heat flow versus UV exposure time under 6 isothermal conditions. Left: $\mathcal{I}_0 = 5$ mW/cm^2. Right: $\mathcal{I}_0 = 10$ mW/cm^2.

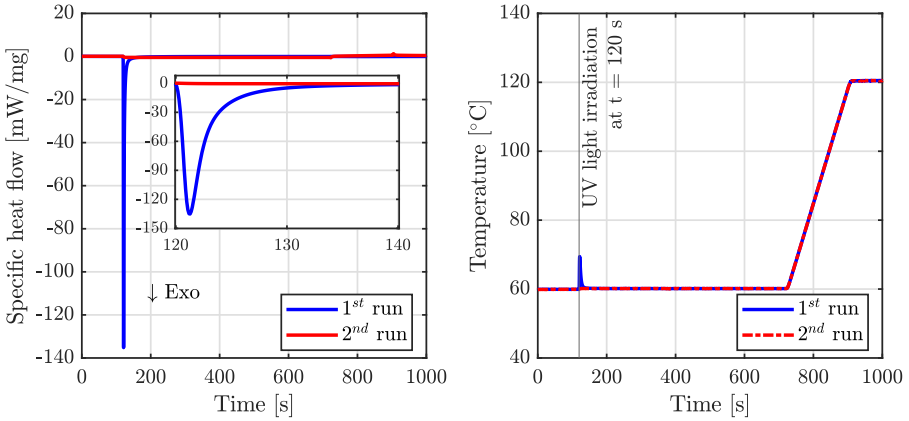

Fig. 9 Photo-DSC measurement for the determination of the total specific heat of reaction h_{tot}. Left: Specific heat flow measurements under the combination of isothermal and non-isothermal conditions with UV light irradiation. Right: Temperature profiles of the measurements.

2.5.2 Specific heat capacity

The specific heat capacity, c_p, is an important parameter if a non-isothermal process such as exothermic reaction during the photopolymerization is considered. According to the standard test method ISO 11537-4, the specific heat capacity of a material is the amount of heat required to increase the temperature by 1 K per unit mass at constant pressure [46]. This definition corresponds to the following equation:

$$c_p = \frac{C_p}{m} = \frac{1}{m}\left(\frac{dQ}{dT}\right)_p \tag{5}$$

m is the mass of material in g, C_p is the heat capacity in J/K with the subscript p indicating an isobaric process and dQ is the amount of heat necessary to raise the temperature of the material by dT.

In the present work, a heat-flux type DSC 214 Polyma was employed for the characterization of the specific heat capacity of PR48 material. Due to their high sensitivity, aluminum crucibles were chosen. The sapphire standard provided by Netzsch was used as the reference sample. Nitrogen was used as a purge with a flow rate of 40 ml/min. DSC scans were performed 3 times for each of the baseline, reference, uncured and almost fully cured ($q = 0.977$) PR48 sample measurements. The desired temperature range is from 10 °C to 60 °C, which is lower than the onset temperature of thermal curing of the liquid photopolymer ($\theta_{onset} > 165$ °C given in Section 2.5.1) and the upper limit of the caloric glass transition which was observed around $\theta = 71.18$ °C in the first heating ramp of the cured sample. Therefore, the two DSC heating runs were performed from 0 °C to 70 °C with a constant heating rate of 5 K/min by applying an isothermal phase of 15 minutes at the start and the end of all measurements.

2.6 Chemical shrinkage

A substantial volumetric shrinkage can lead to distortion of the 3D printed parts. Therefore, curing shrinkage is an important quantity in the photopolymerization process of thermoset resins. The formation of covalent bonds of the crosslinked network increases the molecular packing density. As a result of this crosslinking, the liquid resin is converted into a solid with an increase in density [47]. It is of utmost importance to consider these effects for the modelling of the photopolymerization.

The curing shrinkage measurements presented in this work were carried out following the procedure proposed by Fayolle et al. [48] on the oxidation shrinkage. The volume evolution can be formulated by the variation in mass (m) and density (ρ) as follows:

$$\frac{\Delta V}{V_0} = \frac{\Delta m}{m_0} - \frac{\Delta \rho}{\rho_0} \tag{6}$$

where the indices "0" are assigned to values in the initial state of the physical quantities considered. The value of the Δm is zero since there is no change in mass during the curing reaction.

In order to model the chemical shrinkage as function of the degree of cure, experimental measurements of the variations in mass (m) and density (ρ) were made at ambient temperature to calculate the variation in volume (V) generated during the UV curing using Equation 6. The mass monitoring was carried out by weighing the masses of the samples with different degrees of cure. The masses were measured with an analytical balance MS105DU (Mettler Toledo, Columbus City, OH, USA) with an accuracy of ±0.01 mg. A schematic representation of the experimental setup is illustrated in Figure 10. To record

the change in mass in the liquid due to the fact that a temperature variation leads to a change in the density of the liquid over time, a thermocouple was placed in the bath. Ethanol was utilized as a liquid in the measurement because its density is lower than that of the PR48 liquid resin ($\rho_{PR48} = 1.054$ g/cm^3). The density of the sample was measured first in air and then in ethanol. Mass in ethanol and temperature were recorded for 2 minutes, and the density calculations were made using the data acquired between 30 and 120 seconds, considering the time required for the sample holder to stabilize. A minimum of 0.11% and a maximum of 1.14% change in the sample density and a minimum of $3.635.10^{-5}$ and a maximum of $6.414.10^{-5}$ standard deviation were calculated during these 90-second measurements, and these errors were not correlated with the degree of cure. The density of the sample ρ can be calculated using the following formula [49]:

$$\rho = \frac{m_{sa}}{\alpha(m_{sa} - m_{sl})}(\rho_l - \rho_a) + \rho_a \tag{7}$$

where m_{sa} is the mass of the sample in air, m_{sl} is the mass of the sample in ethanol, ρ_l is the density of ethanol, ρ_a is the density of air (0.0012 g/cm^3 and α is the correction factor (0.99985) given by the manufacturer of the balance that allows for the buoyancy of the holder wire, which is immersed deeper when the sample is placed in the liquid ethanol. During the measurement of the sample mass in ethanol for 2 minutes, it was observed that no mass change occurred within the value that can be read at the resolution of the balance when the calculation was made by considering the density change of the ethanol depending on the temperature.

For the specimen preparation, several samples (30 × 30 × 1 mm^3) were manufactured by curing the liquid resin sandwiched between glass slides separated by Teflon molds in the UV chamber UVP CL-1000L. Three samples were prepared for each UV exposure time of 4, 8, 16, 32, 64, and 1560 minutes. To establish the relationship between the degree of cure and chemical shrinkage in Section 3.5, the residual enthalpy was measured by the DSC to determine the degree of cure of each sample.

3 Results and discussion

3.1 Irradiance characterization

The measurement of the UV energy on the PDMS window as a function of exposure time is illustrated in Figure 11. By applying linear regression, the UV light intensity was calculated as 22.35 mW/cm^2 ($E_0 = 22.35 t_{exp}$) with an R-squared value of 1. Thus, it has been verified that the UV light intensity of the Ember DLP 3D printer is constant over a selected time. Moreover, applying the same approach, a UV light intensity of 19.97 mW/cm^2 was obtained on the glass slide placed on the PDMS window. Table 2 lists the parameters obtained for the irradiance characterization on the different surfaces.

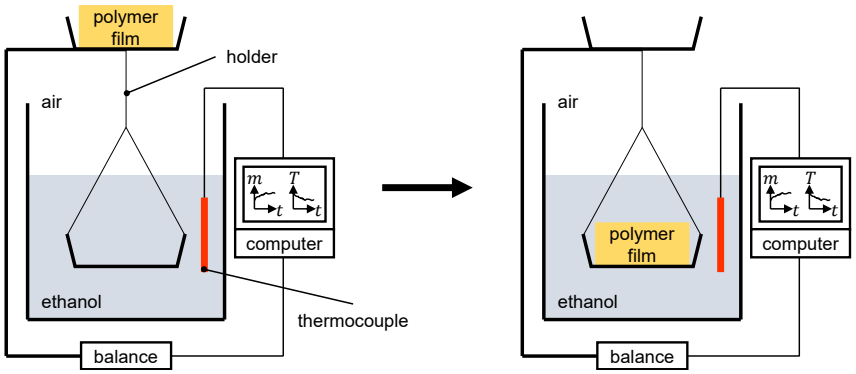

Fig. 10 Experimental setup of measurement of density variation to determine the volumetric shrinkage: mass measurement in air (left) and mass measurement in ethanol (right).

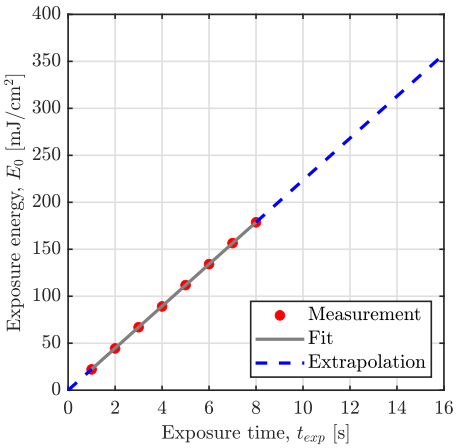

Fig. 11 Relation between the exposure time and UV light energy on the PDMS window of the EMBER 3D DLP printer measured by G&R Labs Model 222 light meter.

Table 2 Irradiance characterization of the Ember DLP 3D printer on different surfaces.

Measurement surface	**PDMS window**	**Glass slide (t = 0.9 mm)**
Irradiance in mW/cm^2	22.35±0.06	19.97±0.03

As for the characterization of the second manufacturing platform, the intensity of the UV light was found to vary from 7.2 to 8 mW/cm^2 over exposure time, according to the measurement technique proposed in Section 2.3. This variation in the UV chamber is not significant for the sample curing because its intensity was not taken into account as input in the sample preparation for chemical shrinkage experiments. The governing parameter is the degree of cure q in both experiments, which was measured by DSC scans.

3.2 Working curve

In order to obtain the UV curing properties of the PR48 photopolymer resin, the results of the SD-OCT scans are plotted using a logarithmically scaled abscissa axis as shown in Figure 12. The resulting curve is referred to as the working curve which is used to calculate the penetration depth D_p and the critical exposure energy E_c using the Jacobs equation given in Equation 3. E_c is the point where the curve intersects the x-axis and D_p is the slope of the curve. Table 3 lists the corresponding values of the two parameters with the R-squared value of 0.991.

Table 3 Parameters of the working curve of the PR48 photopolymer resin.

Parameter	Value	Unit
D_p	223.2±9.6	µm
E_c	30.63±2.41	mJ/cm^2

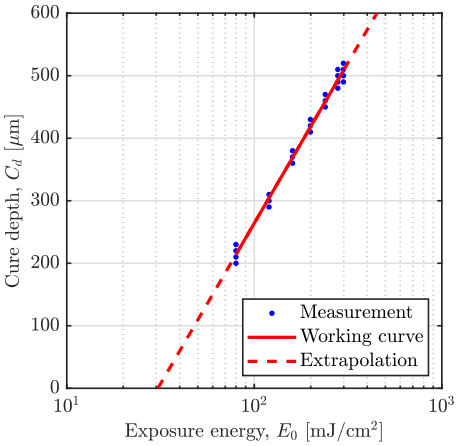

Fig. 12 Working curve of the PR48 photopolymer resin according to Jacobs equation.

3.3 Curing kinetics

The cure rate and degree of cure versus exposure time calculated by Equation 4 are presented in Figures 13 and 14, respectively. As it can be observed, the cure rate and the maximum degree of cure strongly depend on both the temperature and the UV light intensity. Also, the curing rate is larger when light intensity and temperature are higher, particularly at the beginning of the UV irradiation.

In order to model the evolution of the degree of cure, an autocatalytic model is widely used to describe polymerization reaction kinetics [50–52]. Rehbein

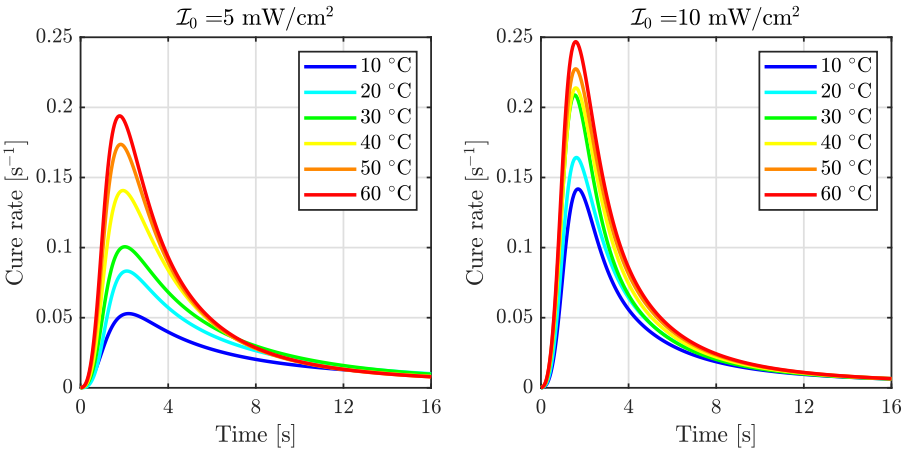

Fig. 13 Measurement of the cure rate $\dot{q}$ versus UV exposure time. Left: $\mathcal{I}_0 = 5$ mW/cm^2. Right: $\mathcal{I}_0 = 10$ mW/cm^2.

et al. [42] applied a phenomenological equation of $(m+n)^{\text{th}}$ order based on the autocatalytic kinetic model of Kamal and Sourour [53, 54] by combining it with the work of Maffezzoli and Terzi [31] to take into account the light intensity [42]. As given in Equation 8, the degree of cure as a function of the UV exposure time t is defined by an ordinary differential equation:

$$\dot{q} = (k_1 + k_2 q^m)\,(q_{\max}(\mathcal{I}, \theta) - q)^n \tag{8}$$

In this model, the degree of cure depends on the time- and location-dependent UV light intensity $\mathcal{I}(z(t), t)$ in mW/cm^2 and the temperature θ in °C. In this equation, k_1 and k_2 denote temperature- and UV light intensity-dependent Arrhenius functions as given in Equation 9:

$$k_i(\mathcal{I}, T) = A_i \exp\left(-\frac{E_i}{RT}\right)\left(\frac{\mathcal{I}}{\mathcal{I}_{ref}}\right)^b \quad i = 1, 2 \tag{9}$$

The parameters E_i are the activation energies, $R = 8.314$ J/(mol.K) is the universal gas constant, T is the absolute temperature in Kelvin, $\mathcal{I}_{ref} = 1$ mW/cm^2 is a reference value to assure the unit consistency of pre-exponential factors A_i, and b is used to fit the experimental data more accurately. Furthermore, $q_{\max}$ represents the temperature- and UV light intensity-dependent maximum attainable degree of cure. Compared to [23], it has been observed that the maximum attainable degree of cure depends not only on the temperature but also on the light intensity, as mentioned in other studies [31, 55, 56]. This dependence on the light intensity has been explained by the position-dependent delay of vitrification in the UV curing thermosetting acrylic system during the reaction [31, 55]. Given the fact that the volumetric change is dependent on the degree of cure, as indicated in Section 3.5, the curing rate also has an effect on the rate of volumetric change. Accordingly, the rate of volumetric

shrinkage falls behind the cure rate of the reaction when the light intensity increases. This difference causes an excess of free volume, resulting in a delayed glass transition of the resin. Depending on the vitrification time measured by DSC, Maffezzoli and Terzi [31] proposed an equation for the $q_{\max}$, and this will be investigated further in the future studies with additional photo-DSC measurements at various UV light intensities. Consequently, Table 4 lists the maximum attainable degrees of cure $q_{\max}$ for 12 measurements.

Table 4 Temperature- and UV light intensity-dependent maximum attainable degree of cure $q_{\max}(\mathcal{I}, \theta)$ for all measurements.

Temperature (°C)	$\mathcal{I}_0 =$ **5 mW/cm²**	$\mathcal{I}_0 =$ **10 mW/cm²**
10	0.635	0.742
20	0.757	0.813
30	0.829	0.872
40	0.893	0.918
50	0.951	0.961
60	0.988	0.996

The curing model given by Equations 8 and 9 contains seven material parameters (A_1, A_2, E_1, E_2, b, m, n) to be identified (see Table 5). The material parameters were obtained by dividing the problem into two parts. Looking at the times $t = 0$ and $t = \infty$, one can obtain two different relations for the initial curing rate and for the maximum attainable degree of cure at $t = \infty$:

$$\begin{aligned} t = 0 \Rightarrow q(0) = 0 \Rightarrow \dot{q}(0) = k_1 q_{\max}^n(\mathcal{I}, \theta) \\ t = \infty \Rightarrow q(\infty) = q_{\max}(\mathcal{I}, \theta) \end{aligned} \tag{10}$$

Using these relations, the first Arrhenius coefficient k_1 and the exponent n of the second reaction were computed by the nonlinear least square fit of Matlab's [57] built-in routine, `lsqnonlin`, with the Levenberg-Marquardt algorithm. A_1, E_1 and b were then obtained from these calculated k_1 coefficients. Following this, the identified parameters were substituted in Equation 8. By applying the initial condition $q(0) = 0$, A_2, E_2 and m were identified with the combination of Matlab's `lsqcurvefit` nonlinear data fitting function in the least-squares sense with the Levenberg-Marquardt algorithm and the `ode45` solver for ordinary differential equations. The optimized parameter set is summarized in Table 5.

The comparison between the experimental measurements and the simulations of the degree of cure according to the curing model defined by Equations 8 and 9 are presented in Figure 14. As can be observed, the proposed model matches the experimental data for all measurement conditions. Furthermore, the photopolymerization reaction, which is dependent on both the temperature and the light intensity, can be mathematically well captured using only 7 model parameters. The model also predicts a significant increase in the degree

Table 5 Identified parameters of the model equation for the degree of cure q.

Parameter	Identified value	Unit	Description
A_1	0.135±0.007	1/s	Pre-exponential factor of the first Arrhenius coefficient
A_2	0.237±0.029	1/s	Pre-exponential factor of the second Arrhenius coefficient
E_1	2003.184±100.159	J/mol	Activation energy of the first Arrhenius coefficient
E_2	2005.08±100.29	J/mol	Activation energy of the second Arrhenius coefficient
m	1.848±0.027	-	Exponent of the first reaction
n	2.2±0.11	-	Exponent of the second reaction
b	0.627±0.031	-	Scaling factor of the influence of the light intensity

of cure following light irradiation, as well as a drop in the curing rate after reaching the peak and an asymptotic evolution stabilizing at $q_{\max}$.

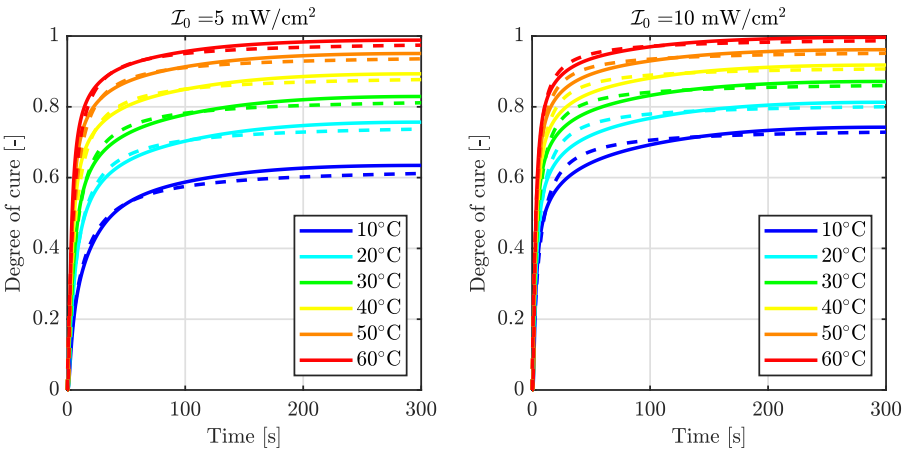

Fig. 14 Measurement (**-**) and simulation (**- -**) of the degree of cure q versus UV exposure time with identified model parameters. Left: $\mathcal{I}_0 = 5$ mW/cm^2. Right: $\mathcal{I}_0 = 10$ mW/cm^2.

3.4 Specific heat capacity

The isobaric specific heat capacity was determined as function of temperature. Figure 15 presents the results of the uncured and almost fully cured PR48 samples. The temperature-dependent specific heat capacities of uncured and cured samples were found to be linear functions of temperature in the range from 10 °C to 110 °C and from 10 °C to 60 °C, respectively. The resulting specific heat capacities were fitted with linear functions given in Equation 11 as proposed by Kolmeder and others [29, 58, 59] where the subscripts "u" and "c" refer to the uncured and the fully cured states of the polymers, respectively. Table 6

summarizes the parameters of the linear equations with their R-squared values. Considering that the specific heat capacities of the uncured and the fully cured PR48 photopolymers are known as function of temperature, a weight-averaged heat capacity function dependent on the degree of cure is proposed in Equation 12 [29].

$$\begin{aligned} c_{p,u}(T) &= A_u T(K) + B_u \\ c_{p,c}(T) &= A_c T(K) + B_c \end{aligned} \tag{11}$$

$$c_p(\theta, q) = c_{p,u}(\theta)(1-q) + c_{p,c}(\theta)q \tag{12}$$

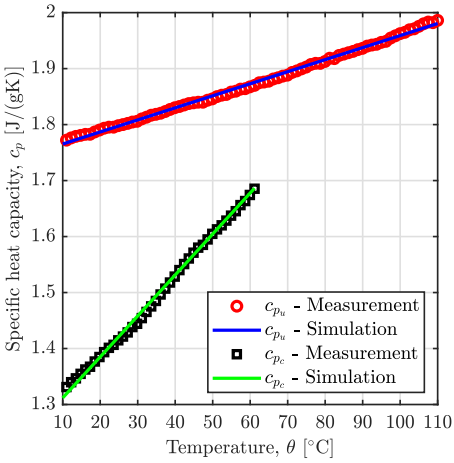

Fig. 15 Simulation of the specific heat capacity of uncured and almost fully cured photopolymer.

Table 6 Identified parameters for the specific heat capacity of uncured and almost fully cured PR48 photopolymer samples.

State	A in J/g	B in J/(gK)	R^2 in [-]
Uncured ($q = 0$)	0.0022	1.1561	1
Cured ($q = 0.977$)	0.0072±0.0001	-0.201±0.0426	0.9964

3.5 Chemical shrinkage

Figure 16 shows the experimental data of the variation in volume of the PR48 material as function of the degree of cure. It is observed that a relationship between the volumetric shrinkage induced by the photopolymerization and the

degree of cure can be expressed by the exponential relationship:

$$\frac{\Delta V}{V_0}(q) = P \exp(Sq) \tag{13}$$

The identified parameters of the model equations are listed in Table 7. It should be remarked that the total volumetric curing shrinkage of PR48 is about 14 %.

Table 7 Identified parameters for the volumetric chemical shrinkage and chemical shrinkage strain.

Parameter	P **in [-]**	S **in [-]**	R^2 **in [-]**
Volumetric shrinkage	$-1.6.10^{-3} \pm 0.8.10^{-3}$	4.611±0.57	0.96

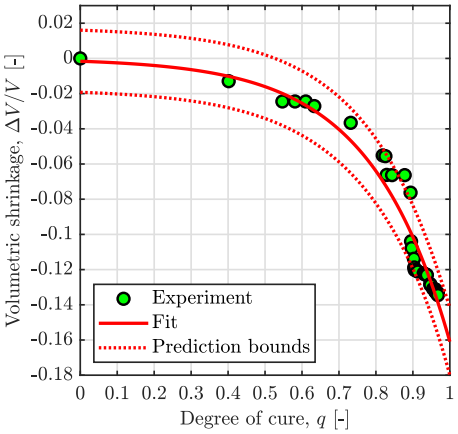

Fig. 16 Volumetric shrinkage of the UV cured samples as a function of degree of cure.

4 Conclusion and perspectives

This work provides a new outlook on the complete quantitative characteristics needed for the prediction of material properties during and after the photopolymerization reaction using experimental methods. UV light intensity measurements were made to characterize the DLP 3D printer and the UV chamber. The UV curing properties of the resin PR48 were determined using the working curve method. Experimental investigation and modelling of the crosslinking reaction was performed by means of photocalorimetric measurements as function of both UV light intensity and temperature. Calorimetric measurements were made to formulate the specific heat capacity as a function of degree of cure and temperature. The chemical shrinkage of the samples

cured at different levels was investigated depending on the degree of cure. Model equations were proposed to predict the material properties based on the degree of cure and the temperature for the UV curing additive manufacturing process.

The results indicate that the photopolymerization rate is significantly affected by the ambient temperature and the UV light intensity; the higher the temperature or the UV light intensity, the faster is the crosslinking reaction and the higher is the degree of cure at the end of the irradiation. In addition, it has been determined that material properties such as chemical shrinkage and specific heat capacity are also strongly dependent on the degree of cure.

In future work, the obtained material database can be exploited to investigate the effect of UV light intensity, temperature and frequency on the viscoelastic properties during and after the photopolymerization process. To optimize the printing process, a finite element (FE) simulation methodology can be implemented by coupling the effects of all relevant physical mechanisms.

Acknowledgments. The financial support of the project "Constitutive modelling of UV-curing printed polymer composites" by the Agence nationale de la recherche (ANR) and the German Research Foundation (DFG) under the grant numbers ANR-18-CE92-0002-01 and LI 696/20-1 is gratefully acknowledged. The authors would also like to thank Dr. Jean-Marc Allain for the optical coherence tomography (OCT) measurements.

References

[1] Bagheri, A., Jin, J.: Photopolymerization in 3D printing. ACS Applied Polymer Materials **1**(4), 593–611 (2019)

[2] Kowsari, K., Akbari, S., Wang, D., Fang, N.X., Ge, Q.: High-efficiency high-resolution multimaterial fabrication for digital light processing-based three-dimensional printing. 3D Printing and Additive Manufacturing **5**(3), 185–193 (2018)

[3] Peng, X., Kuang, X., Roach, D.J., Wang, Y., Hamel, C.M., Lu, C., Qi, H.J.: Integrating digital light processing with direct ink writing for hybrid 3D printing of functional structures and devices. Additive Manufacturing **40**, 101911 (2021)

[4] Zhu, W., Qu, X., Zhu, J., Ma, X., Patel, S., Liu, J., Wang, P., Lai, C.S.E., Gou, M., Xu, Y., Zhang, K., Chen, S.: Direct 3D bioprinting of prevascularized tissue constructs with complex microarchitecture. Biomaterials **124**, 106–115 (2017)

[5] Appuhamillage, G.A., Chartrain, N., Meenakshisundaram, V., Feller, K.D., Williams, C.B., Long, T.E.: 110th anniversary: Vat photopolymerization-based additive manufacturing: Current trends and

future directions in materials design. Industrial & Engineering Chemistry Research **58**(33), 15109–15118 (2019)

[6] Osman, R.B., Alharbi, N., Wismeijer, D.: Build angle: does it influence the accuracy of 3D-printed dental restorations using digital light-processing technology? International Journal of Prosthodontics **30**(2), 182–188 (2017)

[7] Brown, G.B., Currier, G.F., Kadioglu, O., Kierl, J.P.: Accuracy of 3-dimensional printed dental models reconstructed from digital intraoral impressions. American Journal of Orthodontics and Dentofacial Orthopedics **154**(5), 733–739 (2018)

[8] Urrios, A., Parra-Cabrera, C., Bhattacharjee, N., Gonzalez-Suarez, A.M., Rigat-Brugarolas, L.G., Nallapatti, U., Samitier, J., DeForest, C.A., Posas, F., Garcia-Cordero, J.L., Folch, A.: 3D-printing of transparent bio-microfluidic devices in PEG-DA. Lab on a Chip **16**(12), 2287–2294 (2016)

[9] Liu, J., Hwang, H.H., Wang, P., Whang, G., Chen, S.: Direct 3D-printing of cell-laden constructs in microfluidic architectures. Lab on a Chip **16**(8), 1430–1438 (2016)

[10] Gale, B.K., Jafek, A.R., Lambert, C.J., Goenner, B.L., Moghimifam, H., Nze, U.C., Kamarapu, S.K.: A review of current methods in microfluidic device fabrication and future commercialization prospects. Inventions **3**(3), 60 (2018)

[11] Yap, Y.L., Yeong, W.Y.: Additive manufacture of fashion and jewellery products: a mini review. Virtual and Physical Prototyping **9**(3), 195–201 (2014)

[12] Zarek, M., Layani, M., Eliazar, S., Mansour, N., Cooperstein, I., Shukrun, E., Szlar, A., Cohn, D., Magdassi, S.: 4D printing shape memory polymers for dynamic jewellery and fashionwear. Virtual and Physical Prototyping **11**(4), 263–270 (2016)

[13] Zhu, W., Ma, X., Gou, M., Mei, D., Zhang, K., Chen, S.: 3D printing of functional biomaterials for tissue engineering. Current Opinion in Biotechnology **40**, 103–112 (2016)

[14] Zhang, J., Hu, Q., Wang, S., Tao, J., Gou, M.: Digital light processing based three-dimensional printing for medical applications. International Journal of Bioprinting **6**(1) (2020)

[15] Jiang, Y., Wang, Q.: Highly-stretchable 3D-architected mechanical metamaterials. Scientific Reports **6**(1), 34147 (2016)

[16] Patel, D.K., Sakhaei, A.H., Layani, M., Zhang, B., Ge, Q., Magdassi, S.: Highly stretchable and UV curable elastomers for digital light processing based 3D printing. Advanced Materials **29**(15), 1606000 (2017)

[17] Zhu, W., Tringale, K.R., Woller, S.A., You, S., Johnson, S., Shen, H., Schimelman, J., Whitney, M., Steinauer, J., Xu, W., Yaksh, T.L., Nguyen, Q.T., Chen, S.: Rapid continuous 3D printing of customizable peripheral nerve guidance conduits. Materials Today **21**(9), 951–959 (2018)

[18] Mu, Q., Wang, L., Dunn, C.K., Kuang, X., Duan, F., Zhang, Z., Qi, H.J., Wang, T.: Digital light processing 3D printing of conductive complex structures. Additive Manufacturing **18**, 74–83 (2017)

[19] Cullen, A.T., Price, A.D.: Digital light processing for the fabrication of 3D intrinsically conductive polymer structures. Synthetic Metals **235**, 34–41 (2018)

[20] Mendes-Felipe, C., Oliveira, J., Etxebarria, I., Vilas-Vilela, J.L., Lanceros-Mendez, S.: State-of-the-art and future challenges of uv curable polymer-based smart materials for printing technologies. Advanced Materials Technologies **4**(3), 1800618 (2019)

[21] Hwang, H.H., Zhu, W., Victorine, G., Lawrence, N., Chen, S.: 3D-printing of functional biomedical microdevices via light-and extrusion-based approaches. Small Methods **2**(2), 1700277 (2018)

[22] Wu, J., Zhao, Z., Hamel, C.M., Mu, X., Kuang, X., Guo, Z., Qi, H.J.: Evolution of material properties during free radical photopolymerization. Journal of the Mechanics and Physics of Solids **112**, 25–49 (2018)

[23] Rehbein, T., Johlitz, M., Lion, A., Sekmen, K., Constantinescu, A.: Temperature- and degree of cure-dependent viscoelastic properties of photopolymer resins used in digital light processing. Progress in Additive Manufacturing **6**(4), 743–756 (2021)

[24] Chockalingam, K., Jawahar, N., Chandrasekar, U., Ramanathan, K.: Establishment of process model for part strength in stereolithography. Journal of Materials Processing Technology **208**(1-3), 348–365 (2008)

[25] Dizon, J.R.C., Espera Jr, A.H., Chen, Q., Advincula, R.C.: Mechanical characterization of 3D-printed polymers. Additive Manufacturing **20**, 44–67 (2018)

[26] Chen, X., Ashcroft, I.A., Tuck, C.J., He, Y.F., Hague, R.J.M., Wildman, R.D.: An investigation into the depth and time dependent behavior of UV cured 3D ink jet printed objects. Journal of Materials Research **32**(8), 1407–1420 (2017)

[27] Karalekas, D., Aggelopoulos, A.: Study of shrinkage strains in a stereolithography cured acrylic photopolymer resin. Journal of Materials Processing Technology **136**(1-3), 146–150 (2003)

[28] Wu, D., Zhao, Z., Zhang, Q., Qi, H.J., Fang, D.: Mechanics of shape distortion of DLP 3D printed structures during UV post-curing. Soft Matter **15**(30), 6151–6159 (2019)

[29] Tang, Y.: Stereolithography cure process modeling. PhD thesis, School of Chemical & Biomolecular Engineering, Georgia Institute of Technology, Atlanta (August 2005)

[30] Li, Q., Zhou, H., Hoyle, C.E.: The effect of thiol and ene structures on thiol–ene networks: Photopolymerization, physical, mechanical and optical properties. Polymer **50**(10), 2237–2245 (2009)

[31] Maffezzoli, A., Terzi, R.: Effect of irradiation intensity on the isothermal photopolymerization kinetics of acrylic resins for stereolithography. Thermochimica Acta **321**(1-2), 111–121 (1998)

[32] Hong, S.Y., Kim, Y.C., Wang, M., Kim, H.-I., Byun, D.-Y., Nam, J.-D., Chou, T.-W., Ajayan, P.M., Ci, L., Suhr, J.: Experimental investigation of mechanical properties of UV-curable 3D printing materials. Polymer **145**, 88–94 (2018)

[33] Westbeek, S., Remmers, J.J.C., van Dommelen, J.A.W., Maalderink, H.H., Geers, M.G.D.: Prediction of the deformed geometry of vat photopolymerized components using a multi-physical modeling framework. Additive Manufacturing **40**, 101922 (2021)

[34] Arkema - PR48 - Clear Prototyping Material: Technical Data Sheet. Available at https://www.cpspolymers.com/PR48%20TDS.pdf. Accessed: 03/11/2021

[35] Skliutas, E., Kasetaite, S., Jonušauskas, L., Ostrauskaite, J., Malinauskas, M.: Photosensitive naturally derived resins toward optical 3-D printing. Optical Engineering **57**(4), 041412 (2018)

[36] Vallejo-Melgarejo, L.D., Reifenberger, R.G., Newell, B.A., Narváez-Tovar, C.A., Garcia-Bravo, J.M.: Characterization of 3D-printed lenses and diffraction gratings made by DLP additive manufacturing. Rapid Prototyping Journal **25**(10), 1684–1694 (2019)

[37] Hafkamp, T., van Baars, G., de Jager, B., Etman, P.: A feasibility study on process monitoring and control in vat photopolymerization of ceramics. Mechatronics **56**, 220–241 (2018)

[38] Swinehart, D.F.: The Beer-Lambert law. Journal of Chemical Education **39**(7), 333 (1962)

[39] Jacobs, P.F.: Rapid Prototyping & Manufacturing: Fundamentals of Stereolithography. Society of Manufacturing Engineers, Dearborn, MI (1992)

[40] Shah, D.M., Morris, J., Plaisted, T.A., Amirkhizi, A.V., Hansen, C.J.: Highly filled resins for DLP-based printing of low density, high modulus materials. Additive Manufacturing **37**, 101736 (2021)

[41] Schindelin, J., Arganda-Carreras, I., Frise, E., Kaynig, V., Longair, M., Pietzsch, T., Preibisch, S., Rueden, C., Saalfeld, S., Schmid, B., Tinevez, J.Y., White, D.J., Hartenstein, V., Eliceiri, K., Tomancak, P., Cardona, A.: Fiji: an open-source platform for biological-image analysis. Nature Methods **9**(7), 676–682 (2012)

[42] Rehbein, T., Lion, A., Johlitz, M., Constantinescu, A.: Experimental investigation and modelling of the curing behaviour of photopolymers. Polymer Testing **83**, 106356 (2020)

[43] Xiang, H., Yin, J., Lin, G., Liu, X., Rong, M., Zhang, M.: Photo-crosslinkable, self-healable and reprocessable rubbers. Chemical Engineering Journal **358**, 878–890 (2019)

[44] Brady, G.A., Halloran, J.W.: Differential photo-calorimetry of photopolymerizable ceramic suspensions. Journal of Materials Science **33**, 4551–4560 (1998)

[45] Jiang, F., Drummer, D.: Curing kinetic analysis of acrylate photopolymer for additive manufacturing by photo-DSC. Polymers **12**(5), 1080 (2020)

[46] ISO Standard 11357-4: Plastics — Differential scanning calorimetry (DSC) — Part 4: Determination of specific heat capacity. Technical report, International Organization for Standardization, Geneva, CH (June 2014)

[47] Hossain, M., Chatzigeorgiou, G., Meraghni, F., Steinmann, P.: A multi-scale approach to model the curing process in magneto-sensitive polymeric materials. International Journal of Solids and Structures **69-70**, 34–44 (2015)

[48] Fayolle, B., Audouin, L., George, G.A., Verdu, J.: Macroscopic heterogeneity in stabilized polypropylene thermal oxidation. Polymer Degradation and Stability **77**(3), 515–522 (2002)

[49] Mettler Toledo: NewClassic Balances MS-S/MS-L Models, Operating

Instructions

[50] Hossain, M., Possart, G., Steinmann, P.: A small-strain model to simulate the curing of thermosets. Computational Mechanics **43**(6), 769–779 (2009)

[51] Golaz, B., Michaud, V., Leterrier, Y., Månson, J.-A.E.: UV intensity, temperature and dark-curing effects in cationic photo-polymerization of a cycloaliphatic epoxy resin. Polymer **53**(10), 2038–2048 (2012)

[52] Leistner, C., Hartmann, S., Abliz, D., Ziegmann, G.: Modeling and simulation of the curing process of epoxy resins using finite elements. Continuum Mechanics and Thermodynamics **32**(2), 327–350 (2020)

[53] Kamal, M.R.: Thermoset characterization for moldability analysis. Polymer Engineering & Science **14**(3), 231–239 (1974)

[54] Sourour, S., Kamal, M.R.: Differential scanning calorimetry of epoxy cure: isothermal cure kinetics. Thermochimica Acta **14**(1-2), 41–59 (1976)

[55] Esposito Corcione, C., Greco, A., Maffezzoli, A.: Photopolymerization kinetics of an epoxy-based resin for stereolithography. Journal of Applied Polymer Science **92**(6), 3484–3491 (2004)

[56] Halloran, J.W.: Ceramic stereolithography: additive manufacturing for ceramics by photopolymerization. Annual Review of Materials Research **46**, 19–40 (2016)

[57] Matlab Online Documentation. Available at https://www.mathworks.com/help/. Accessed: 03/11/2021

[58] Kolmeder, S., Lion, A., Landgraf, R., Ihlemann, J.: Thermophysical properties and material modelling of acrylic bone cements used in vertebroplasty. Journal of thermal analysis and calorimetry **105**(2), 705–718 (2011)

[59] Nawab, Y., Tardif, X., Boyard, N., Sobotka, V., Casari, P., Jacquemin, F.: Determination and modelling of the cure shrinkage of epoxy vinylester resin and associated composites by considering thermal gradients. Composites Science and Technology **73**, 81–87 (2012)